JOURNAL OF AGRICULTURAL AND FOOD CHEMISTRY

Photocatalytic Ozonation of Winery Wastewaters

OLGA GIMENO, F. JAVIER RIVAS,* FERNANDO J. BELTRÁN, AND MARÍA CARBAJO

Departamento de Ingeniería Química y Química Física, Facultad de Ciencias, Universidad de Extremadura, Edificio Jose Luis Sotelo, Avenida de Elvas S/N, 06071 Badajoz, Spain

The combination of UV-A/vis radiation and ozone, in the presence of titanium dioxide, has been investigated as a potential destructive technology for the treatment of winery wastewaters. The contribution of the adsorption stage, single ozonation, photolytic ozonation, and photocatalysis has previously been assessed. Adsorption onto the TiO_2 surface accounts for a 15–20% removal of the initial chemical oxygen demand (COD). The rest of the subsystems attain COD conversion values in the range of 37–43%. The photocatalytic ozonation of the effluent, under the operating conditions investigated, increases the COD depletion to a value close to 80%. The working pH was studied in the range of 3–11, the optimum value being located in the acidic region (pH 3). A saturation-like behavior is experienced when the amount of TiO_2 used is varied in the interval of 0–3 g L^{-1}. Contrary to the use of ozone alone, the system UV-A/vis/O_3/TiO_2 leads to the total mineralization of the COD removed. A proposed pseudoempirical model suggested the existence of a synergistic effect when radiation, ozone, and titanium dioxide are combined.

KEYWORDS: Titanium dioxide; ozone; adsorption; photocatalysis; winery wastewater

INTRODUCTION

Winemaking is one of the most important agricultural activities in Mediterranean countries. Thus, Spain, France, and Italy account for 14.85, 11.2, and 10.66% of the total area of vineyards in the world, respectively (*1*). Vineyards in the world cover approximately 7.9×10^6 ha. The wine industry generates a seasonal effluent characterized by a high organic load from the different stages taking place in wine production. According to Vlyssides et al. (*2*), the generated wastewater is distributed after completion of the following steps: first reception of grapes (around September), wastewater from washing operations; second, must production, similarly to the previous stage, wastewater is primarily formed in washing practices; third, fermentation, which does not involve effluent generation; fourth, decanting, contaminated waters arise from cleaning and wine transportation to maturation–stabilization tanks, which constitutes the fifth stage; sixth, wine is filtered and once more wastewater is produced in washing and transport operations; finally, wine is sold or bottled in the seventh stage. The highest wastewater production takes place during the second and sixth stages, accounting for >50% of the total effluent produced. The variability in composition and flow of the winery wastewaters involves the appearance of serious difficulties in terms of considering the biodegradation as a suitable technology to treat these effluents (*3*). Additionally, the presence of a high concentration of phenol type compounds also prevents the use of traditional aerobic bioprocesses to handle these effluents.

Chemical oxidation technologies based on the application of visible radiation constitute a promising tool to deal with problematic wastewaters. Thus, the use of titanium dioxide in UV-A/vis-based photocatalytic processes has been recognized as an attractive process to oxidize organic molecules. The mechanism behind the oxidation includes the photogeneration of electron–hole pairs in the surface of the catalyst and the formation of hydroxyl radicals by combination of holes and adsorbed water molecules. In aerated systems, electrons can be trapped by oxygen to finally yield peroxy radicals.

The primary advantages of photocatalysis are the availability of solar radiation and cheapness and stability of the photocatalyst (titanium dioxide). Among the drawbacks, the difficult separation of fine particles of TiO_2 from the aqueous matrix and the wastage of radiation after electron–hole recombination can be listed. To overcome the first inconvenience, coating of TiO_2 particles onto reactor surfaces or pellets has been proposed (*4*). In the second case, an excess of oxygen or addition of inorganic peroxides might prevent the wastage of light (*5*). Inorganic peroxides are capable of trapping electrons and simultaneously generate more free radicals. Similarly, ozone can accept electrons from the conduction band leading to formation of the ozonide radical, which finally yields hydroxyl radicals. Photocatalytic ozonation is presented, therefore, as a powerful oxidizing system involving two main direct routes of degradation, namely, direct ozonation and photolysis and at least four paths for HO° generation according to

$$O_3 + e^- \rightarrow O_3^{o-} \rightarrow HO_3^o \rightarrow HO^o + O_2 \quad (1)$$

$$O_3 + OH^- \rightarrow HO_2^o + O_2^{o-} \rightarrow HO_3^o + O_2 \rightarrow HO^o + 2O_2 \quad (2)$$

* Corresponding author (telephone +0034924289385; e-mail fjrivas@unex.es; fax +0034924289385).

10.1021/jf072167i CCC: $37.00
Published on Web 10/26/2007

$$TiO_2 + h\nu \rightarrow e^- + h^+ \xrightarrow{H_2O} HO^o + H^+ \quad (3)$$

$$O_3 + h\nu \rightarrow H_2O_2 \rightarrow 2HO^o \quad (4)$$

The majority of works focused on the use of ozone in photocatalytic processes have dealt with pure model compounds, paying little attention to the application of this technology to real effluents (*6*).

In this work, a comparative study of different advanced oxidation technologies, including the photocatalytic ozonation of a real winery wastewater, has been conducted. Additionally, an attempt has been made to model the different processes taking place.

MATERIALS AND METHODS

Wastewater was collected from a wine industry located in Almendralejo (province of Badajoz, southwestern Spain). The characterization of this effluent led to the following parameters: chemical oxygen demand (COD) = 9250 ± 380 ppm; biological oxygen demand (BOD) = 7100 ± 654 ppm; pH 7.1 ± 0.4; and total phenolic content (as gallic acid) = 268 ± 33 ppm. Prior to its use, wastewater was diluted with tap water to obtain an effluent with an initial COD concentration in the range of 800 ± 100 ppm. Dilution of effluents to fulfill the regulatory laws of discharge is a common practice in small–medium wine industries, where the investment needed to implement an anaerobic process is not economically feasible. In other cases, advances in wine technology allow for the generation of relatively lowly contaminated effluents in the proximity of 1000 ppm of COD.

Titanium dioxide (TiO_2) P25 from Degussa was used as adsorbent/photocatalyst with no previous treatment. According to the manufacturer, Degussa P25 is a nonporous solid formed by the combination of the anatase (70%) and rutile (30%) forms of titanium dioxide. The solid is characterized by the following properties: density, 3.8 g cm^{-3}; BET surface area, 50 m^2 g^{-1}; average primary particle, 30 nm; pH in aqueous solution, 3–4.

A 1 L capacity tubular borosilicate glass photoreactor (450 mm long, 80 mm diameter) was used in all of the experiments. Oxidation of wastewater was conducted at atmospheric pressure in 0.85 L of the aqueous solution.

Ozonation experiments were carried out by means of a mixture of ozone and oxygen fed through a porous diffuser. Ozone was produced from oxygen in a laboratory SANDER 301.7 ozone generator with a maximum capacity of 12 g h^{-1}.

When light was used, the reactor walls were insulated to avoid release of radiation and/or heat outside. Prior to the photodegradation experiments, the suspension was stirred for 60 min in the dark to achieve the adsorption equilibrium. Oxygen was continuously fed into the water bulk by means of a diffuser.

A high-pressure mercury lamp (Heraeus, TQ 718 700 W) immersed in a Pyrex glass well was placed at the middle of the reactor. The lamp bandwidth was located in the range of 238–579 nm with three main wavelengths emitting at 254, 313, and 366 nm. UV-B radiation was cut off by Pyrex glass. Temperature was partially controlled by a jacket around the glass well in which water was circulated; nevertheless, this parameter could not be adequately maintained due to the excess heat released by the lamp. Incident radiation photon fluxes at 313 and 366 nm were 0.189 and 0.331 einstein h^{-1}, respectively, and the corresponding radiation powers were 20.1 and 30.0 W, respectively. A detailed description of the experimental setup can be found elsewhere (*7*).

When TiO_2 (Degussa P25) was added, the solid was maintained in suspension by magnetic stirring.

Analyses were carried out in triplicate, and average results are shown in the figures. COD was determined in a Dr. Lange spectrophotometer, the method being based on the standard dichromate reflux method (*8*). BOD was measured following the procedure of the Warburg respirometer (*9*). For this purpose, nonacclimated microorganisms from the municipal wastewater plant of the city of Badajoz were used. Because microorganisms in the environment are not acclimated to any specific effluent, use of nonacclimated microorganisms in BOD tests results in a less biased analysis. To assess the degree of mineralization, total organic carbon (TOC) was determined by a Shimazdu TOC 5000A analyzer by directly injecting the aqueous solution.

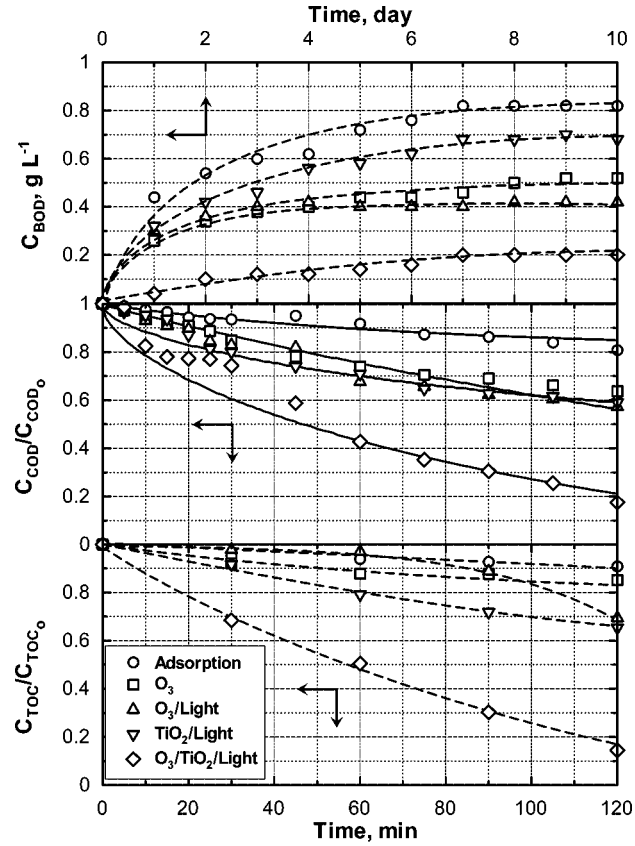

Figure 1. Treatment of winery wastewaters by means of different oxidative and nonoxidative processes. Experimental conditions: $C_{TiO_2}o = 1.5$ g L^{-1}, $C_{O_3}g_{inlet} = 50$ mg L^{-1}, pH 7, $C_{COD_o} = 0.8$ g L^{-1} (average value), $C_{TOC_o} = 0.3$ g L^{-1}, $Q = 50$ L h^{-1}, $T = 293$ K. Solid lines correspond to COD model calculations.

RESULTS AND DISCUSSION

Comparison of Oxidation Systems. A series of experiments was carried out to assess the efficiency of the following processes: adsorption, ozonation, photolytic ozonation, photocatalysis, and photocatalytic ozonation. **Figure 1** shows the results obtained in terms of normalized COD and TOC removal and BOD evolution.

As observed from this figure, adsorption of organic/inorganic molecules by titanium dioxide accounts for roughly 20% of the initial COD load and approximately 10% of organic carbon. Consequently, it is suggested that some inorganic molecules contributing to COD are trapped by the catalyst. If ozone is applied with a concentration of 50 mg L^{-1}, the final COD conversion increases to 37%, whereas the mineralization level is located around 15%. The combinations light/O_3 and light/TiO_2 do not achieve significantly better results in terms of COD removal (43 and 41%, respectively); however, the mineralization degree increases to values close to those reported for COD depletion (31 and 35%, respectively). Finally, if the most sophisticated system is applied, that is, the combination of ozone, titanium dioxide, and radiation, the results are significantly improved. Thus, COD is reduced to 17% of its initial value, whereas the reduction in TOC follows a parallel trend with a

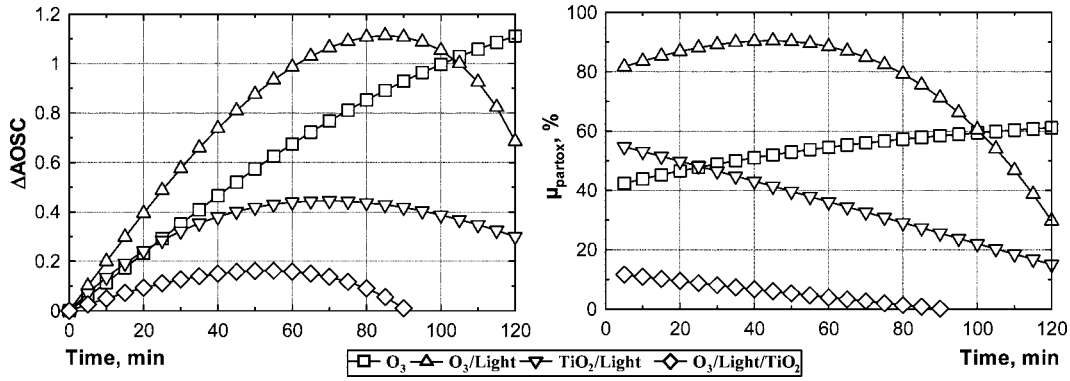

Figure 2. Treatment of winery wastewaters by means of different oxidative processes. Evolution of the average oxidation state of carbon increment and partial oxidation yield with time. Experimental conditions: $C_{TiO_{2_0}} = 1.5$ g L^{-1}, $C_{O_3g_{inlet}} = 50$ mg L^{-1}, pH 7, $C_{COD_0} = 0.8$ g L^{-1} (average value), $C_{TOC_0} = 0.3$ g L^{-1}, $Q = 50$ L h^{-1}, $T = 293$ K.

remaining 15%; that is, by considering the analytical error, practically all of the organic material oxidized has been simultaneously mineralized. This degree of mineralization is not experienced for the rest of the systems. To assess the mineralization efficacy of the different oxidation processes used, the following described parameters were calculated. On the one hand, there is the average oxidation state of carbon (AOSC) and its increment (ΔAOSC). The average oxidation state of carbon may suffer modifications from the minimum possible value (−4 for methane) to the maximum value (+4 for carbon dioxide). The two parameters (COD and TOC are expressed in molar units, whereas the subscript "o" indicates initial conditions) are defined as (*10*)

$$\mathrm{AOSC} = \frac{4(\mathrm{TOC} - \mathrm{COD})}{\mathrm{TOC}} \tag{5}$$

$$\Delta\mathrm{AOSC} = \frac{4(\mathrm{TOC} - \mathrm{COD})}{\mathrm{TOC}} - \frac{4(\mathrm{TOC_o} - \mathrm{COD_o})}{\mathrm{TOC_o}} = 4\left(\frac{\mathrm{COD_o}}{\mathrm{TOC_o}} - \frac{\mathrm{COD}}{\mathrm{TOC}}\right) \tag{6}$$

On the other hand, the partial oxidation yield (*11*) (COD and TOC in ppm) is described by eqs 7 and 8. The values of μ_{partox} are in the interval of 0–1 for total mineralization or no mineralization occurring in the process, respectively.

$$\mu_{partox} = \frac{\mathrm{COD_{partox}}}{\mathrm{COD_o} - \mathrm{COD}} \tag{7}$$

$$\mathrm{COD_{partox}} = \left(\frac{\mathrm{COD_o}}{\mathrm{TOC_o}} - \frac{\mathrm{COD}}{\mathrm{TOC}}\right)\mathrm{TOC} \tag{8}$$

$\mathrm{COD_{partox}}$ indicates the fraction of COD removed not leading to CO_2 and water. As observed in **Figure 2**, different trends are experienced depending on the oxidation system used. Hence, single ozonation is the only process during which the average oxidation state of carbon continuously increases, suggesting the accumulation of oxygenated species. As a consequence, the fraction of COD removal not leading to carbon dioxide and water also increases incessantly from 40 to 60% throughout the reaction period. If light is applied, the low initial TOC removal attained in the first 70–80 min of oxidation involves a sharp increase of oxygenated intermediate accumulation. Thereafter, probably when a sufficient amount of radicals have been generated, TOC undergoes an abrupt decrease, leading to a change in the slope of the ΔAOSC and μ_{partox} toward a negative value. In this sense μ_{partox} shows an initial value of 80% leveling off to roughly 30% at the end of the reaction. The photocatalysis and photocatalytic ozonation are the best options in terms of mineralization efficiency. In the first case, there is a rise of approximately 0.4 unit in the ΔAOSC along the whole process, whereas the mineralization fraction continuously increases from the start of the photocatalysis. In the second case, the oxidation state of carbon practically does not change during the oxidation. Additionally, the accumulation of oxygenated species into the reaction media is also quite low, presenting μ_{partox} values close to 0 after 60 min of reaction. After 90 min of reaction, the trends in COD and TOC are so close that some anomalous values are obtained for μ_{partox}; for instance, this parameter attains slight negative values, likely due to the error associated with COD and TOC analysis (the minimum value should be 0).

The biodegradability of contaminated effluents is normally enhanced if complex molecules are broken into smaller oxygenated compounds. However, in some cases, the intermediates formed retain some biotoxic nature and prevent the adequate biological treatment. According to the first statement, from **Figure 2**, ozone and the photolytic ozonation should lead to an effluent more biodegradable than the photocatalytic process. For instance, in the three systems the reduction in COD was similar but mineralization was more pronounced in the photocatalytic process. **Figure 1C** illustrates how the intial guess does not occur and how the TiO_2/light process leads to the effluent with a higher value of BOD. The reasons seems to rely on the second idea previously stated; that is, intermediates formed in the O_3 and O_3/light systems are likely more biorecalcitrant than those obtained in the TiO_2/light system. The case of the photocatalytic ozonation is not comparable to the previous processes because in the latter, the depletion of COD and TOC was significantly higher. Nevertheless, if the biodegradability of an effluent is considered to be directly related to the ratio BOD/COD, the values obtained for the O_3, light/O_3, light/TiO_2, and O_3/light/TiO_2 systems are 1.0, 0.9, 1.8, and 1.7, respectively. Values of the BOD/COD ratio above 1.0 indicate endogenous respiration of microorganizms due to the low ratio $\mathrm{COD_{(biodegradable)}}$/microorganisms. In all cases the treated wastewater shows the minimum requirements to be finally disposed into the public sewage system (COD < 500 ppm). The photocatalytic ozonation effluent can even be discharged into natural aquatic environments as it presents a COD value below 160 ppm.

Once the efficiency of the process O_3/light/TiO_2 has been demonstrated, the influence of two primary operating variables must be investigated, namely, catalyst concentration and pH.

Photocatalytic Ozonation System. *Catalyst Concentration Influence.* **Figure 3** depicts the data obtained after completion

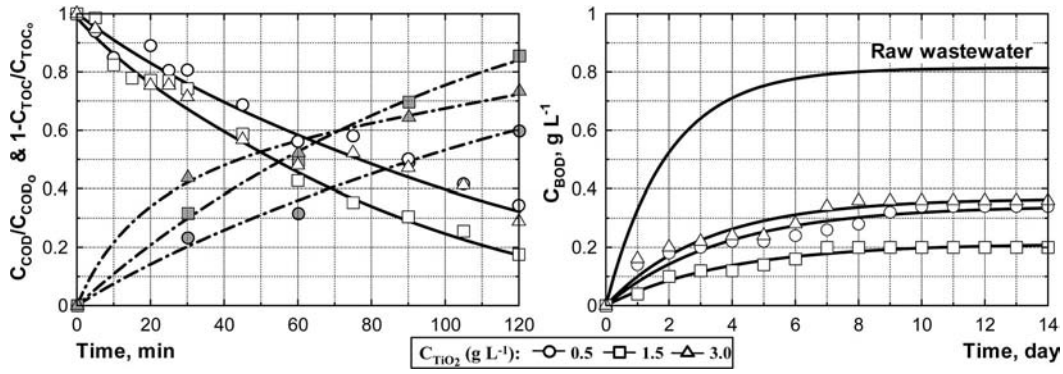

Figure 3. Treatment of winery wastewaters by means of photocatalytic ozonation. Experimental conditions: $C_{O_3}g_{inlet} = 50$ mg L^{-1}, pH 7, $C_{COD_o} = 0.8$ g L^{-1} (average value), $C_{TOC_o} = 0.3$ g L^{-1}, $Q = 50$ L h^{-1}, $T = 293$ K. Solid symbols correspond to TOC conversion.

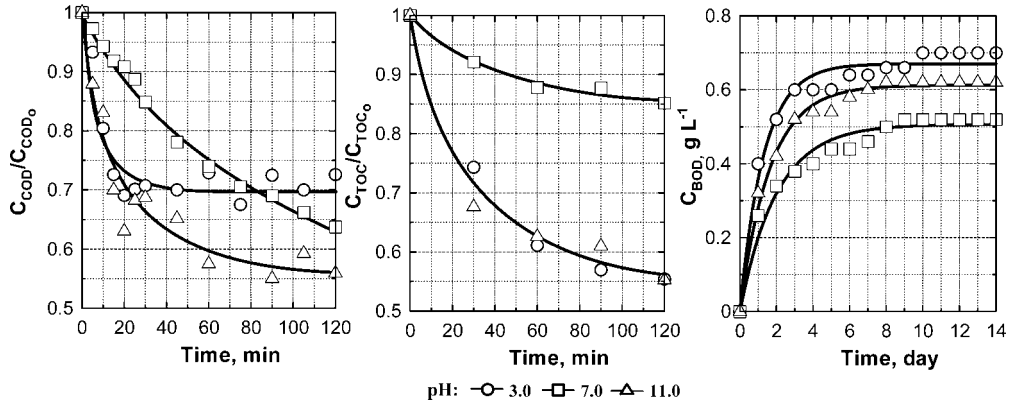

Figure 4. Treatment of winery wastewaters by single ozonation. Experimental conditions: $C_{O_3}g_{inlet} = 50$ mg L^{-1}, $C_{COD_o} = 0.8$ g L^{-1} (average value), $C_{TOC_o} = 0.3$ g L^{-1}, $Q = 50$ L h^{-1}, $T = 293$ K.

of a series of three experiments with different photocatalyst concentrations. As inferred from this plot, catalyst load seems to exert a negligible influence on the final results attained.

Thus, the experiments conducted with 0.5 and 3.0 g L^{-1} of the catalyst result in the same COD conversion after 120 min of treatment. It seems that the run completed with the highest catalyst concentration shows a faster initial conversion, particularly in terms of TOC removal. This behavior could be attributed to a higher extent of the adsorption stage; however, the excess of catalyst used provokes a shielding effect in the emitted radiation, slowing the kinetics of the process after 30–40 min. From **Figure 3**, it seems that under the operating conditions used, the optimum in catalyst concentration is located around 1.5 g L^{-1}. Similar results have been reported in the case of the hydrogen peroxide promoted photocatalysis of a mixture of three phenols (*7*).

The biodegradability of the effluent also presents an optimum corresponding to a concentration of 1.5 g L^{-1} of TiO_2. Thus, BOD curves can be fitted to an equation of the type

$$C_{BOD} = C_{BOD_f}[1 - \exp(-kt)] \quad (9)$$

where C_{BOD_f} is the steady state final value of BOD achieved and k is a kinetic related parameter. Fitting of data in **Figure 3** to expression 9 led to C_{BOD_f} values of 0.34, 0.21, and 0.37 g L^{-1} and k values of 0.27, 0.26, and 0.31 min^{-1} for runs conducted with 0.5, 1.5, and 3.0 g L^{-1} of TiO_2, respectively. As inferred from these parameters, there are no significant kinetic differences in biodegradability of the three effluents. Determination of the ratio C_{BOD_f}/COD_f gave values of 1.3, 1.7, and 1.4 (once more endogenous respiration is envisaged).

In all experiments, ozone at the gas outlet was immediately detected after the reaction started, suggesting the development of chemically controlled processes. Steady state concentrations of ozone gas outlet were achieved in approximately 20 min with values approaching the 84, 81, and 95% of the ozone inlet concentration fed to the reactor for increasing values of catalyst load. Thus, it is confirmed the highest ozone uptake in the experiment carried out with 1.5 g L^{-1} of TiO_2 and the lowest ozone utilization observed for the run completed with 3.0 g L^{-1} of TiO_2.

pH Influence. The effect of pH in the photocatalytic ozonation was checked in the interval 3–11. To discriminate between the pH influence in the single ozonation and in the O_3/light/TiO_2 system, the corresponding blank runs were conducted in the absence of any radiation and catalyst. **Figure 4** illustrates the results obtained.

From the single ozone evolution profiles observed in **Figure 4** it can be stated that pH 11 slightly enhances the COD removal if compared to neutral or acidic conditions (i.e., ozone is catalytically decomposed by hydroxyl anions, see Kinetic Considerations). In the latter case, after an initial fast removal of easily oxidizable compounds, COD depletion profiles come to a halt, likely due to accumulation of ozone recalcitrant compounds. The evolution of TOC is similar, although stripping of carbonates and formed CO_2 at acidic pH involves a similar efficiency at pH values 3 and 11.

The effect of proton concentrations in the O_3/light/TiO_2 system is displayed in **Figure 5**. Unlike single ozonation, the optimum pH for the photocatalytic ozonation of the winery wastewaers is located in the acidic region. Contrarily, the worst results are obtained under alkaline conditions (especially in terms of mineralization level achieved). Several reasons can be enumerated:

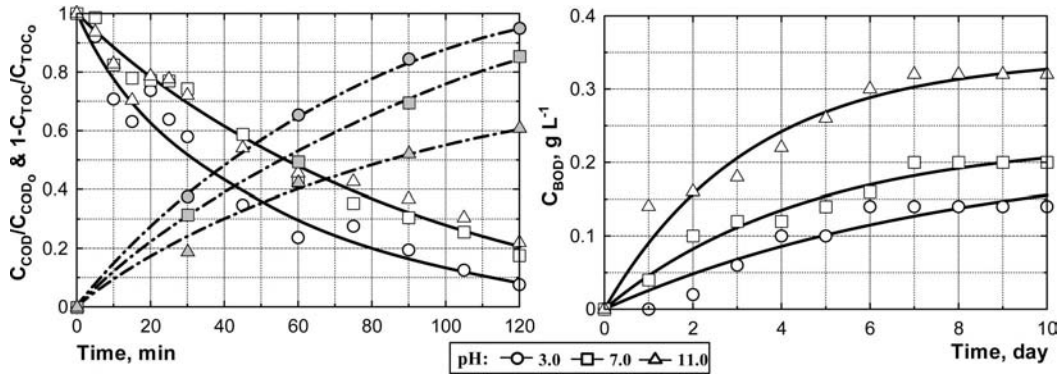

Figure 5. Treatment of winery wastewaters by means of photocatalytic ozonation. Experimental conditions: $C_{O_3g_{inlet}} = 50$ mg L^{-1}, $C_{COD_o} = 0.8$ g L^{-1} (average value), $C_{TOC_o} = 0.3$ g L^{-1}, $C_{TiO_{2o}} = 1.5$ g L^{-1}, $Q = 50$ L h^{-1}, $T = 293$ K. Solid symbols correspond to TOC conversion.

Adsorption of contaminants onto TiO_2 surfaces is a key step in photocatalytic processes; this step is normally favored at low pH values.

At high pH, ozone is rapidly decomposed by OH^-. As a consequence, the role played by the O_3 molecule in terms of electron trapping and electron–hole recombination is reduced.

Carbonates do accumulate at pH 11, leading to the corresponding efficacy decrease in TOC removal.

Kinetic Considerations. To ascertain the potential synergistic effect of coupling ozone, radiation, and titanium dioxide, a simplistic kinetic study has been conducted by separately analyzing each subsystem. This kinetic study is just aimed at discriminating between the different contributions in the phototcatalytic ozonation; it does not claim to be an exhaustive detailed mechanism of actual reactions taking place. The following stages were therefore proposed:

Adsorption. The kinetics of the adsorption stage was simulated by a simple driving force involving free adsorption active sites and dissolved COD (*12*):

$$COD_{(solution)} + TiO_{2(solid)} \xrightarrow{k_{Ads}} COD_{(absorbed)} \qquad (10)$$

$$-\frac{dC_{COD}}{dt} = k_{Ads} C_{COD} C_{free\ sites} \qquad (11)$$

The concentration of free adsorption active sites is hypothesized to be the difference between its initial concentration and those adsorption sites already occupied by COD. Taking into account that the initial amount of free adsorption sites is proportional to initial TiO_2 concentration and the occupied sites are proportional to adsorbed COD, eq 11 leads to

$$-\frac{dC_{COD}}{dt} = k_{Ads} C_{COD}\left(\alpha C_{TiO_2} - \beta\frac{C_{COD_o} - C_{COD}}{C_{TiO_2}}\right) \qquad (12)$$

After rearrangement

$$-\frac{dC_{COD}}{dt} = k_{Ads} C_{COD}[\alpha C_{TiO_2} - \gamma(C_{COD_o} - C_{COD})] = k'_{Ads} C_{COD}\left[\frac{\alpha}{\gamma} C_{TiO_2} - (C_{COD_o} - C_{COD})\right] \qquad (13)$$

with

$$\gamma = \frac{\beta}{C_{TiO_2}} \quad \text{and} \quad k'_{Ads} = \frac{k_{Ads}}{\gamma} \qquad (14)$$

Considering the final equilibrium value for COD and the amount of TiO_2 used (0.019 M), a value of $\alpha/\gamma = 0.27$ was calculated. The rate constant in eq 13, $k_{Ads} \approx 0.51 \pm 0.06$ M^{-1} min^{-1}, was obtained from the adsorption experiment by minimizing the expression

$$\text{error} = \frac{1}{N}\sum_{i=1}^{i=N}\frac{(C_{COD_{calcd}} - C_{COD_{exptl}})^2}{C_{COD_{exptl}}} \qquad (15)$$

where the subscripts calcd and exptl stand for calculated and experimental values, respectively. Model calculations are displayed in **Figure 1A**.

Ozonation. The immediate appearance of ozone at the gas outlet suggests that ozonation proceeds in the slow regimen. The classic ozonation mechanism was used in this case by setting the COD evolution as the target parameter. For so doing, the ozone mass transfer between the liquid and gas phases and the following radical set of reactions were considered:

dissolved ozone:

$$\frac{dC_{O_3}}{dt} = k_L a\left(\frac{C_{O_3g_{outlet}} RT}{H} - C_{O_3}\right) + r_{O_3} \qquad (16)$$

ozone in the gas phase:

$$\frac{dC_{O_3g_{outlet}}}{dt} = (C_{O_3g_{inlet}} - C_{O_3g})\frac{Q_g}{(1-\beta)V} - k_L a\left(\frac{C_{O_3g_{outlet}} RT}{H} - C_{O_3}\right)\frac{\beta}{1-\beta} \qquad (17)$$

where $k_L a$ is the overall volumetric mass transfer coefficient of the liquid phase, R is the universal gas constant, T is the temperature, H is Henry's constant calculated for pure water by using the equation of Sotelo et al. (*13*), β is the liquid holdup (assumed value of 0.99), Q_g is the gas flow rate, and V is the reaction volume. Additionally, r_{O_3} accounts for those ozone-consuming reactions in the liquid phase.

radical reactions (k units in moles, liters, and seconds):

$$O_3 + OH^- \rightarrow HO_2^o + {}^oO_2^- \quad k = 70 \qquad (18)$$

$$O_3 + {}^oO_2^- \rightarrow O_2 + {}^oO_3^- \quad k = 1.6\times10^9 \qquad (19)$$

$$H^+ + {}^oO_3^- \rightleftarrows HO_3^o \quad k = 2.0\times10^{10}, k^- = 3.7\times10^4 \qquad (20)$$

$$HO_3^o \rightarrow O_2 + HO^o \quad k = 5.0\times10^4 \qquad (21)$$

$$O_3 + HO^o \rightleftarrows HO_4^o \quad k = 2.0\times10^9, k^- = 1.0\times10^2 \qquad (22)$$

$$HO_4^o \rightarrow O_2 + HO_2^o \quad k = 2.8\times10^4 \tag{23}$$

$$(H_2O) + {}^oO_3^- \rightleftarrows HO_3{}^o + OH^- \quad k = 54.2,\ k^- = 1.0\times10^{10} \tag{24}$$

$$HO_2^- + O_3 \rightarrow HO^o + {}^oO_2^- + O_2 \quad k = 2.8\times10^6 \tag{25}$$

$$HO_2{}^o \rightleftarrows H^+ + {}^oO_2^- \quad k = 3.2\times10^5, k^- = 2.0\times10^{10} \tag{26}$$

$$H_2O_2 \rightleftarrows H^+ + HO_2^- \quad k = 4.5\times10^{-2}, k^- = 2.0\times10^{10} \tag{27}$$

$$H^+ + OH^- \rightleftarrows H_2O \quad k = 1.0\times10^{11}, k^- = 1.0\times10^{-3} \tag{28}$$

$$H_2O_2 + HO^o \rightarrow HO_2^o + H_2O \quad k = 3.3\times10^7 \tag{29}$$

Additionally, the removal of COD and the first intermediates by molecular ozone and HO° has been added to the mechanism. Given the high content in phenol type compounds, the first attack of HO° radicals to COD has been assumed to lead to the formation of a new molecule of hydroxyl radicals. In this sense, Han and co-workers reported a significant increase of OH° occurrence after ozone decomposition in the presence of some phenol derivatives and 5,5-dimethylpyrrolidine 1-oxyl (DMPO) as the radical trapping agent. The mechanism would develop through formation of an organic peroxy radical. Thus, after the HO° abstraction reaction, the formed organic radical would instantaneously trap a molecule of oxygen, releasing thereafter a new HO° molecule and forming the corresponding ketone (*12*).

$$O_3 + COD \rightarrow COD_{ox} \quad k = ? \tag{30}$$

$$O_3 + COD_{ox} \rightarrow CO_2 + H_2O \quad k = ? \tag{31}$$

$$HO^{3O} + COD \rightarrow COD_{ox} + HO^o \quad k = ? \tag{32}$$

$$HO^o + COD_{ox} \rightarrow CO_2 + H_2O \quad k = ? \tag{33}$$

The two direct ozonation rate constants were obtained by minimizing the differences between predicted and actual COD concentrations (see **Figure 1A**). Values for *k* in eqs 32 and 33 were given general values of 5.0×10^9 and 0.5×10^9 M^{-1} s^{-1}, respectively (*15*). The ozonation rate constants obtained in eqs 30 and 31 were similar, in the range of 35–40 M^{-1} s^{-1}. To corroborate the kinetic regimen taking place, the Hatta number was calculated, leading to a value of 0.15, which is below 0.3 that is the upper limit for the reaction to develop in the slow regimen.

Photolytic ozonation. As seen in **Figure 1A**, in this particular case, the combination of O_3 and UV-A/vis light did not exert any significant changes in the COD profile if compared to that experienced in the single ozonation. Accordingly, this subsystem was not considered in the simulation process (it is well described by the single ozonation).

Photocatalysis. This system involves, a priori, the adsorption of contaminants (already modeled), the formation of hydroxyl radicals onto the TiO_2 surface, and the oxidation of adsorbed COD with surface HO°:

$$TiO_2\text{-}HO^o_{(surface)} + COD_{(adsorbed)} \rightarrow HO^o + CO_2 + H_2O \quad k = ? \tag{34}$$

Given the high mineralization level achieved in this system, no intermediates have been considered to be formed in eq 34.

Because radiation intensity and oxygen/water excess were always maintained under the operating conditions used, the TiO_2-$HO°_{(surface)}$ formation rate has been assumed to be proportional to TiO_2 concentration:

$$\frac{dC_{TiO_2\text{-}HO^o_{(surface)}}}{dt} = kC_{TiO_2} \tag{35}$$

The rate constant in eq 35 was given a value of $(8.0 \pm 0.4) \times 10^{-7}$ s^{-1} after fitting of experimental and calculated COD data points (**Figure 1A**).

Photocatalytic Ozonation. Finally, to ascertain the potential synergistic effect of the combination of ozone and photocatalysis, the previous single stages were considered with no additional reactions. After the set of first-order ordinary differential equations had been solved, the theoretical COD profile obtained underestimated the actual removal rate of this parameter. As a consequence, it can be hypothesized that additional reactions have to be included to account for the effect observed. The new step introduced into the mechanism included the formation of the ozonide radical after ozone reaction with electrons at the photocatalyst surface (reaction 1). Thereafter, the ozonide radical instantaneously generates a HO° surface molecule. This reaction has been presupposed to be proportional to TiO_2 and dissolved ozone concentration.

$$\frac{dC_{O_3{}^{o-}}}{dt} = \frac{dC_{TiO_2-HO^o_{(surface)}}}{dt} = kC_{TiO_2}C_{O_3} \tag{36}$$

After fitting of experimental data, the reaction rate in eq 36 was given a value of 0.5 ± 0.03 M^{-1} s^{-1}.

Figure 6 shows a plot of the modeled COD conversion profiles obtained through reactions eqs 10–36 and the experimental COD conversion data points. R^2 values calculated for the straight lines in **Figure 6** are 0.97 in all cases except the adsorption process ($R^2 = 0.91$), indicating an acceptable simulation of results.

Dissolved ozone analysis is a complicated task in aqueous solutions in which a solid is present. As a consequence, the data obtained in this measurement should be taken with caution. In any case, the proposed model is also capable of acceptably simulate C_{O3} profiles with time for the first 30 min of reaction; thereafter dissolved ozone experimentally suffers a sharp decrease, whereas the calculated values show a slight increasing trend. Differences between model and empirical data can be

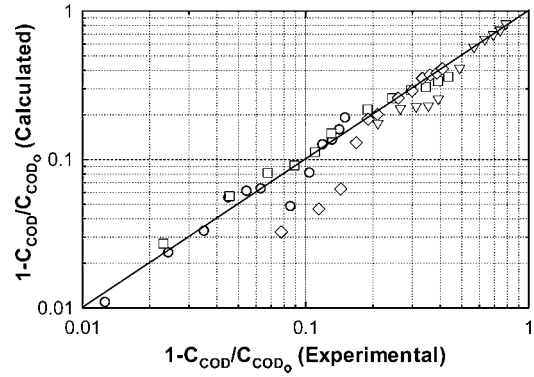

Figure 6. Modeling of the photocatalytic ozonation of winery wastewaters. Conditions and symbols are as in **Figure 1**.

attributed to a number of causes, that is, analytical errors, lack of ozone-consuming reactions (for instance, ozone photolysis), etc. In any case, the model achieves its main task, for instance, the direct comparison between systems regarding the elimination of the target COD. The model used in this investigation can be considered acceptable for the range of operating variables used. The possibilities of completing more experiments under different conditions include, for instance, the use of different lamps; however, in this case some adjustable parameters should be recalculated (i.e., a different lamp should modify the generation of surface hydroxyl radicals).

ACKNOWLEDGMENT

We thank Jaume Weichsel from Degussa Iberia S.A. (Spain) for a complimentary sample of titania P-25 powder.

Nomenclature

αproportionality constant in eqs 12 and 13, dimensionless
β proportionality constant in eq 12, mol L^{-1}
γconstant defined in eq 14, dimensionless
μ_{partox}partial oxidation yield, dimensionless
AOSC average oxidation state of carbon, dimensionsless
BODbiological oxygen demand, mg of O_2 L^{-1}
calcdcalculated value
$C_i$concentration of species *i*, mol L^{-1}
CODchemical oxygen demand, mg of O_2 L^{-1}
COD_{partox}COD removal not leading to CO_2 and H_2O, mg of O_2 L^{-1}
exptlexperimental value
ffinal value
*H*Henry's constant, mol L^{-1} atm^{-1}
βliquid holdup, dimensionless
*k*rate constant
$k_La$overall volumetric mass transfer coefficient of the liquid phase, s^{-1}
*N*total number of samples
Oinitial conditions
$Q_g$gas flow rate, m^3 s^{-1}
*R*universal gas constant, atm L mol^{-1} K^{-1}
*T*temperature, K
TOCtotal organic carbon, mg of O_2 L^{-1}
*V*reaction volume, m^3

LITERATURE CITED

(1) http://www.winesfromspain.com, accessed July 2007.
(2) Vlyssides, A. G.; Barampouti, E. M.; Mai, S. Wastewater characteristics from Greek wineries and distilleries. *Water Sci. Technol.* **2005**, *51*, 53–60.
(3) Navarro, P.; Sarasa, J.; Sierra, D.; Esteban, S.; Ovelleiro, J. L. Degradation of wine industry wastewaters by photocatalytic advanced oxidation. *Water Sci. Technol.* **2005**, *51*, 113–120.
(4) Hosseini, S. N.; Borghei, S. M.; Vossoughi, M.; Taghavinia, N. Immobilization of TiO_2 on perlite granules for photocatalytic degradation of phenol. *Appl. Catal. B: Environ.* **2007**, *74*, 53–62.
(5) Gimeno, O.; Carbajo, M.; López, M. J.; Melero, J. A.; Beltrán, F.; Rivas, F. J. Photocatalytic promoted oxidation of phenolic mixtures: An insight into the operating and mechanistic aspects. *Water Res.* **2007**,in press.
(6) Agustina, T. E.; Ang, H. M.; Vareek, V. K. A review of synergistic effect of photocatalysis and ozonation on wastewater treatment. *J. Photochem. Photobiol. C: Photochem. Rev.* **2005**, *6*, 264–273.
(7) Gimeno, O.; Carbajo, M.; Beltrán, F. J.; Rivas, F. J. Phenol and substituted phenols AOP's remediation. *J. Haz. Mater.* **2005**, *B119*, 99–108.
(8) APHA. *Standard Methods for the Examination of Water and Wastewater*, 19th ed.; American Public Health Association: New York, 1995.
(9) Means, J. L.; Anderson, S. J. Comparison of five different methods for measuring biodegradability in aqueous environments. *Water, Air Soil Pollut.* **1981**, *16*, 301–305.
(10) Rivas, F. J.; Beltraìn, F. J.; Gimeno, O.; Acedo, B. Wet air oxidation of wastewater from olive oil mills. *Chem. Eng. Technol.* **2001**, *24*, 415–421.
(11) Hellenbrand, R.; Mantzavinos, D.; Metcalfe, I. S.; Livingston, A. G. Integration of wet oxidation and nanofiltration for treatment of recalcitrant organics in wastewater. *Ind. Eng. Chem. Res.* **1997**, *36*, 5054–5062.
(12) Rivas, F. J.; Beltrán, F. J.; Gimeno, O.; Carbajo, M. Fluorene oxidation by coupling of ozone, radiation, and semiconductors: a mathematical approach to the kinetics. *Ind. Eng. Chem. Res.* **2006**, *45*, 166–174.
(13) Sotelo, J. L.; Beltran, F. J.; Benitez, F. J.; Beltran-Heredia, J. Henry's law constant for the ozone–water system. *Water Res.* **1989**, *23*, 1239–1246.
(14) Han, S.; Ichikawa, K.; Utsumi, H. Quantitative analysis for the enhancement of hydroxyl radical generation by phenols during ozonation in water. *Water Res.* **1998**, *32*, 3261–3266.
(15) Buxton, G. V.; Greenstock, C. L.; Helman, W. P.; Ross, A. B. Critical review of rate constants for reactions of hydrated electrons, hydrogen atoms and hydroxyl radicals in aqueous solution. *J. Phys. Chem. Ref. Data* **1988**, *17*, 513–886.

Received for review July 19, 2007. Revised manuscript received September 20, 2007. Accepted September 24, 2007. This work has been supported by the MEC of Spain and the European Region Development Funds of the European Commission (Project CTQ2006-04745/PPQ). O.G. (Ramón y Cajal contract) and M.C. (FPU grant) also thank the Spanish Ministry of Science and Education.

JF072167I